Path-reversed photoelectron diffraction from surfaces: Composite layer treatment

H. C. Poon,[1] M. D. Pauli,[1] A. Wander,[2] and D. K. Saldin[1]
[1]*Department of Physics and Laboratory for Surface Studies, University of Wisconsin–Milwaukee, P.O. Box 413, Milwaukee, Wisconsin 53201*
[2] *CLRC Daresbury Laboratory, Daresbury, Warrington, WA4 4AD, United Kingdom*
(Received 27 September 2001; published 27 March 2002)

A computational scheme for photoelectron diffraction, based on a path-reversal formalism, is developed for crystal surfaces with many atoms per unit cell. We show that the computation may be performed efficiently by simple modification to a computer program developed earlier for low-energy electron diffraction. We show that the results are essentially indistinguishable from those from conventional forward-path calculations. Overall agreement with experimental data from different samples for a MgO(001) surface is also found.

DOI: 10.1103/PhysRevB.65.134115 PACS number(s): 61.14.Qp, 61.14.Dc

I. INTRODUCTION

In core-level photoemission, an electron wave is excited from the initial state of an emitting atom and travels through the surface to the detector. A Green's-function formalism for an ordered slab that follows these multiple-scattering processes forward in time was previously reported.[1,2] There is also a renewed interest in this problem for photoemission from clusters and disordered structures.[3–6] Recently, an alternative approach based on the reciprocity theorem was proposed.[7] In this approach, the electron is propagated backward from the detector to the emitter. Wave amplitudes at different emitters can be found with just a single run of the algorithm. In contrast, in the usual forward propagation approach a separate multiple-scattering calculation is repeated for each emitter and each initial state. Since the later approach is based on essentially path-reversed low-energy electron diffraction (LEED), any code developed for LEED may easily be modified to include the photon-electron coupling at the final stage. The path-reversed method was initially implemented by a modification of the tensor LEED program of Rous and Pendry,[8] which handled just surfaces capable of being modeled by layers consisting of primitive two-dimensional (2D) lattices. That paper described simulations of Auger diffraction patterns from a Cu(001) surface, where excellent agreement was found for both low and high photoelectron energies. The present paper extends this treatment to photoelectron diffraction, and to surfaces modeled by planes containing more than a single atom per layer unit cell. Although the present application is to a periodic surface, an adaptation of the method to a representation of the sample by a nonperiodic cluster of atoms is quite straightforward. Thus the idea is potentially useful even for the modeling of photoelectron diffraction from disordered surfaces and nanocluster structures.

If the scattered wave function between layers of a surface is expandable into plane waves, algorithms like the renormalized forward scattering (RFS) method[9,10] may be applied to find efficiently the wave amplitudes incident on either side of each layer. When the spacing between layers is small, the plane-wave expansion may not converge well. For such cases, it is appropriate to combine layers with small interlayer spacings into a single composite layer, and to calculate the scattering *within* the composite layer in a spherical-wave basis, while retaining the plane-wave expansion for scattering *between* composite layers. This hybrid scheme is known as the *combined-space method*.[10]

In Sec. II, we will show how a path-reversed photoelectron diffraction calculation may be performed by a modification of the LEED combined-space method. Section III describes the results of calculations by this method of the photoelectron diffraction from a MgO(001) surface. The results are compared with those from forward-propagation methods and with experimental data. Section IV contains our conclusions.

II. THEORY

In angle-resolved photoemission, the amplitude $C(\mathbf{k}_\parallel)$ of the measured signal may be characterized by $\mathbf{k}_\parallel$, the component parallel to the sample's surface of the wave vector of the wave entering the detector, namely,

$$C(\mathbf{k}_\parallel)=\langle \mathbf{k}_\parallel | G\Delta | \phi_i \rangle, \tag{1}$$

where G is the Green's function for the electron's propagation from the emitter to the detector, Δ is the photon-electron interaction Hamiltonian, and $|\phi_i\rangle$ represents the ith core-electron state. Inserting complete sets of eigenvectors of positions $\mathbf{r}$ and $\mathbf{r}'$, we may write this as

$$\begin{aligned} C(\mathbf{k}_\parallel) &= \int\int \langle \mathbf{k}_\parallel | \mathbf{r}' \rangle \langle \mathbf{r}' | G | \mathbf{r} \rangle \langle \mathbf{r} | \Delta | \mathbf{r} \rangle \langle \mathbf{r} | \phi_i \rangle d\mathbf{r}' d\mathbf{r} \\ &= \int \left[\int \langle \mathbf{r} | G | \mathbf{r}' \rangle \langle \mathbf{r}' | -\mathbf{k}_\parallel \rangle d\mathbf{r}' \right] \Delta(\mathbf{r}) \langle \mathbf{r} | \phi_i \rangle d\mathbf{r}. \end{aligned} \tag{2}$$

The last equality follows from the reciprocity theorem,

$$\langle \mathbf{r} | G | \mathbf{r}' \rangle = \langle \mathbf{r}' | G | \mathbf{r} \rangle, \tag{3}$$

and $\Delta(\mathbf{r})$ is diagonal with respect to the position eigenvectors. The theorem is valid even if the potential is taken to be complex to represent the effects of inelastic scattering.

The Green's function (G) may be written

$$\langle \mathbf{r}|G|\mathbf{r}'\rangle = G(\mathbf{r},\mathbf{r}') = G^o(\mathbf{r},\mathbf{r}') + \int G^o(\mathbf{r},\mathbf{r}_1)T(\mathbf{r}_1,\mathbf{r}_2) \times G^o(\mathbf{r}_2,\mathbf{r}')d\mathbf{r}_1 d\mathbf{r}_2. \quad (4)$$

Thus the term within square brackets in Eq. (2) may be written

$$\langle \mathbf{r}|G|-\mathbf{k}_\parallel\rangle = \langle \mathbf{r}|G^o|-\mathbf{k}_\parallel\rangle + \langle \mathbf{r}|G^oTG^o|-\mathbf{k}_\parallel\rangle. \quad (5)$$

The free-space Green's function in the plane wave representation is[11]

$$G^o(\mathbf{r},\mathbf{r}') = \frac{1}{8\pi^3}\int d^3k' \frac{e^{-i\mathbf{k}'\cdot(\mathbf{r}-\mathbf{r}')}}{E-\frac{k'^2}{2}-i\epsilon} = \frac{i}{\mathcal{A}}\sum_{\mathbf{k}'_\parallel}\frac{e^{-i\mathbf{k}'.(\mathbf{r}-\mathbf{r}')}}{k'_z} \quad \text{for} \quad z>z', \quad (6)$$

where $\mathcal{A}$ is the normalization area:

$$\langle \mathbf{r}|G^o|-\mathbf{k}_\parallel\rangle = \frac{1}{\mathcal{A}}\int G^o(\mathbf{r},\mathbf{r}')\exp(-i\mathbf{k}_\parallel\cdot\mathbf{r}')\delta(z')d\mathbf{r}' = \frac{i}{\mathcal{A}}\frac{e^{-i\mathbf{k}\cdot\mathbf{r}}}{k_z} \quad \text{for} \quad z>z'. \quad (7)$$

This may be regarded as a plane wave of wave vector $-\mathbf{k}$ (with a component parallel to the surface of $-\mathbf{k}_\parallel$) incident directly on an atom in the vicinity of $\mathbf{r}$. As for the second term in Eq. (5), this represents the wave that reaches the vicinity of the same atom after all possible scattering processes with all atoms of the sample.

The quantity $\langle \mathbf{r}|G|-\mathbf{k}_\parallel\rangle$ may be calculated by means of a LEED computer program for an incident plane wave $\exp(-i\mathbf{k}\cdot\mathbf{r}')$. Specifically, the program can calculate the coefficients of a spherical-wave representation of this wave field, namely,

$$\langle \mathbf{r}|G|-\mathbf{k}_\parallel\rangle = \frac{i}{k_z\mathcal{A}}\sum_L A_{jL}j_l(k|\mathbf{r}-\mathbf{r}_j|)Y_L(\mathbf{r}-\mathbf{r}_j), \quad (8)$$

where j_l is a spherical Bessel function of order l, Y_L is a spherical harmonic of angular momentum quantum numbers $L=(l,m)$, and

$$A_{jL} = \sum_{nL'}(1-G^ot)^{-1}_{jL,nL'}4\pi i^{l'}Y^*_{L'}(-\hat{\mathbf{k}})e^{-i\mathbf{k}\cdot\mathbf{R}_n}, \quad (9)$$

where t is an atomic t matrix. The amplitudes A_{jL} represent incoming spherical waves at the position of the jth emitter after the path-reversed incident plane wave is multiply scattered by the atoms n of the sample. On a muffin-tin model, the total radial wave function just outside the emitter may be written $j_l(k|\mathbf{r}-\mathbf{r}_j|)+t_lh_l(k|\mathbf{r}-\mathbf{r}_j|)$, where $t_l=(e^{2i\delta_l}-1)/2$ and δ_l is the atomic phase shift of angular momentum l. The effects of atomic vibration at a finite temperature on the phase shifts can be calculated in the usual way.[9] Each wave matches onto the function $e^{i\delta_l}R_l(k|\mathbf{r}-\mathbf{r}_j|)$ inside the muffin tin, where $R_l(k|\mathbf{r}-\mathbf{r}_j|)$ is the regular solution of angular momentum quantum number l of the radial Schrödinger equation for the jth atom. Therefore, inside the emitter we have

$$\langle \mathbf{r}|G|-\mathbf{k}_\parallel\rangle = \frac{i}{k_z\mathcal{A}}\sum_L A_{jL}e^{i\delta_l}R_l(k|\mathbf{r}-\mathbf{r}_j|)Y_L(\mathbf{r}-\mathbf{r}_j). \quad (10)$$

For a periodic composite layer with N atoms per unit cell, it is convenient to decompose the scattering paths into multiple-scattering processes among N subplanes, each being a primitive 2D lattice with just a single atom per unit cell. In other words, the expansion $t+tG^ot\ldots$ of the inverse in Eq. (9) can be written as $\tau+\tau G^o\tau+\cdots$, where $\tau=t+tG^ot\ldots$ may be thought of as a renormalized atomic t matrix which incorporates all multiple-scattering paths within a single subplane.

The calculation of the amplitudes (9) involves summations within a subplane of the form:

$$(1-G^ot)^{-1}e^{-i\mathbf{k}\cdot\mathbf{R}_n} = e^{-i\mathbf{k}\cdot\mathbf{R}_j} + G^o_{ji}te^{-i\mathbf{k}\cdot\mathbf{R}_i}+\ldots + G^o_{ji}t\cdots tG^o_{mn}te^{-i\mathbf{k}\cdot\mathbf{R}_n}, \quad (11)$$

where the lattice vector $\mathbf{R}_n$ indicates the position of atom n within the subplane. Note that the general term can be rearranged in the form

$$G^o_{ji}t\cdots te^{-i\mathbf{k}\cdot\mathbf{R}_m}(G^o_{mn}e^{i\mathbf{k}\cdot(\mathbf{R}_m-\mathbf{R}_n)})t. \quad (12)$$

As G^o_{mn} depends only on the relative position $\mathbf{R}_m-\mathbf{R}_n$, we may write this as

$$G^o_{ji}t\cdots te^{-i\mathbf{k}\cdot\mathbf{R}_m}G^{intra}t, \quad (13)$$

where

$$G^{intra} = \sum_{\mathbf{P}\neq 0}G(\mathbf{P})e^{i\mathbf{k}\cdot\mathbf{P}} \quad (14)$$

is the intralayer propagator. Since each subplane is a primitive lattice, the difference between two lattice vectors is also a lattice vector $\mathbf{P}$. Hence the sum is over all lattice points except the origin in the subplane. Applying the same argument to other factors to the left in Eq. (13), we may write this term as

$$e^{-i\mathbf{k}\cdot\mathbf{R}_j}G^{intra}t\cdots G^{intra}t, \quad (15)$$

and hence Eq. (11) can be summed to yield

$$e^{-i\mathbf{k}\cdot\mathbf{R}_j}(1-G^{intra}t_j)^{-1}, \quad (16)$$

and the effective scattering factor of an atom in subplane j is

$$\tau_j = t_j(1-G^{intra}t_j)^{-1}. \quad (17)$$

A similar argument suggests that the amplitudes of the spherical waves incident on the origin atom in subplane j, after initial incidence on subplane j' and subsequent multiple scattering between the subplanes, is

$$(1-G^{inter}\tau)^{-1}_{jj'}e^{-i\mathbf{k}\cdot\mathbf{R}_{j'}}, \quad (18)$$

where the elements of the interlayer propagator matrices, $G^{inter}_{j,j'}$ are

$$G^{inter}_{jL_1,j'L_2}=\sum_{\mathbf{P}} G_{L_1L_2}(\mathbf{r}_{jj'}+\mathbf{P})e^{-i\mathbf{k}\cdot\mathbf{P}}, \tag{19}$$

where the quantity $\mathbf{r}_{jj'}$ is the interlayer vector between subplanes j and j'. Hence Eq. (9) may be rewritten to give the final amplitude incident on the origin atom in layer j after further multiple scattering among the atoms of the same subplane,

$$A_{jL}=\sum_{j',L',L''}(1-G^{intra}t_j)^{-1}_{LL'} \times(1-G^{inter}\tau)^{-1}_{jL',j'L''}4\pi i^{l''}Y^*_{L''}(\mathbf{k})e^{-i\mathbf{k}\cdot\mathbf{R}_{j'}}, \tag{20}$$

where j and j' are subplane indices.

Substituting Eq. (20) into Eq. (10) gives an expression for the total wave function $\langle\mathbf{r}|G|-\mathbf{k}_\parallel\rangle$ finally incident onto the photoemitter after the multiple scattering of the backpropagated photoelectron wave. Substitution of the resulting expression into Eq. (2) gives

$$C(\mathbf{k}_\parallel)=\int\langle\mathbf{r}|G|-\mathbf{k}_\parallel\rangle\Delta(\mathbf{r})\langle\mathbf{r}|\phi_i\rangle d\mathbf{r} =\frac{i}{k_z\mathcal{A}}\sum_L(-)^m e^{i\delta_l}A_{\bar{L}}M^{ij}_L, \tag{21}$$

where

$$M^{ij}_L=\int R_l(k|\mathbf{r}-\mathbf{r}_j|)Y^*_L(\mathbf{r}-\mathbf{r}_j)\Delta\psi_i(\mathbf{r})d\mathbf{r}, \tag{22}$$

using the result $Y_L=(-1)^mY^*_{\bar{L}}$, where $\bar{L}=(l,-m)$, and replacing the dummy index m with $-m$ under the summation over L. By the selection rule for atomic photoemission, $l=l_i\pm1$ and $m=m_i$.

The transition rate is given by[11]

$$\frac{dw}{d\Omega}(\mathbf{k}_\parallel)=\frac{\mathcal{A}^2}{4\pi^2}k^{out}(k^{out}_z)^2|C(\mathbf{k}_\parallel)|^2. \tag{23}$$

Note that the factor of $\mathcal{A}$ in Eq. (21) cancels those in Eq. (23), and the expression for the transition rate is in fact independent of $\mathcal{A}$.

The above treatment assumes all atoms of the surface combined into one giant composite layer. In practice, it is usually more efficient to divide the surface into a set of composite layers with the wave field between the layers expanded into a plane-wave representation. The amplitudes $B^{(+)}_{\mathbf{g},q}$ and $B^{(-)}_{\mathbf{g},q+1}$ of plane waves of wave vectors $K^{(+)}_{\mathbf{g}}$ and $K^{(-)}_{\mathbf{g}}$ respectively, incident on layer q from above and below, respectively (where the components of these wave vectors parallel to the layers differ by the 2D reciprocal-lattice vectors $\mathbf{g}$ of the layers) may be calculated by a standard RFS scheme in a LEED computer program. In this case the spherical-wave amplitudes A_{jL} will need to be calculated by a sum of terms of the form of Eq. (20), each of which is multiplied by the amplitudes $B^{(+)}_{\mathbf{g},q}$ and $B^{(-)}_{\mathbf{g},q+1}$ and which has the vector $-\mathbf{k}$ in Eq. (20) replaced by $K^{(+)}_{\mathbf{g}}$ and $K^{(-)}_{\mathbf{g}}$, respectively.

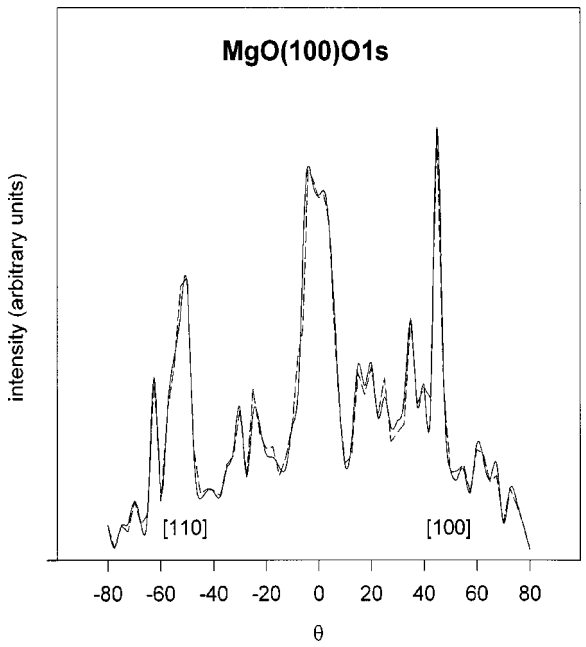

FIG. 1. Comparison of calculated O 1s photoelectron diffraction polar angle distributions along the [100] and [110] azimuths from a MgO(001) surface using the path-reversed algorithm described in the text (dotted line) and a conventional algorithm that traces the path of the photoelectron from emitter to detector (solid line).

III. NUMERICAL RESULTS AND DISCUSSION

Figure 1 shows calculated photoelectron diffraction intensities as a function of polar angle along azimuths [100] and [110], originating at O 1s atomic core electron states from a MgO(001) surface which is assumed to be bulk terminated.[12,13] The calculation using the path-reversed algorithm was performed for a stack of five-composite layers, each composite layer consisting of a subplane of magnesium and a subplane of oxygen atoms. The combined-space method is necessary here because the two subplanes are coplanar. The usual LEED package and RFS method[10] were employed for scattering between composite layers. As a matter of fact, the scattering matrices of a composite layer in LEED are proportional to $\Sigma_{j,L}e^{-i\mathbf{k}_f\cdot\mathbf{R}_j}Y_L(\mathbf{k}_f)t_{jl}A_{jL}$, where A_{jL} is given by Eq. (20) and $\mathbf{k}_f$ is the direction of the scattered wave. Modifications were made in only one of the subroutines that calculates the scattering matrices of a composite layer. Both the atomic matrix elements and phase shifts are calculated from a potential constructed using the program MUFPOT.[9]

For comparison, the same photoelectron diffraction intensities were also calculated by the usual time-forward scheme[11] with the MgO(001) surface, modeled instead by a single composite layer of ten subplanes. Excellent agreement is found with the results of the path-reversed calculations. It should be noted that, although the forward-propagation cal-

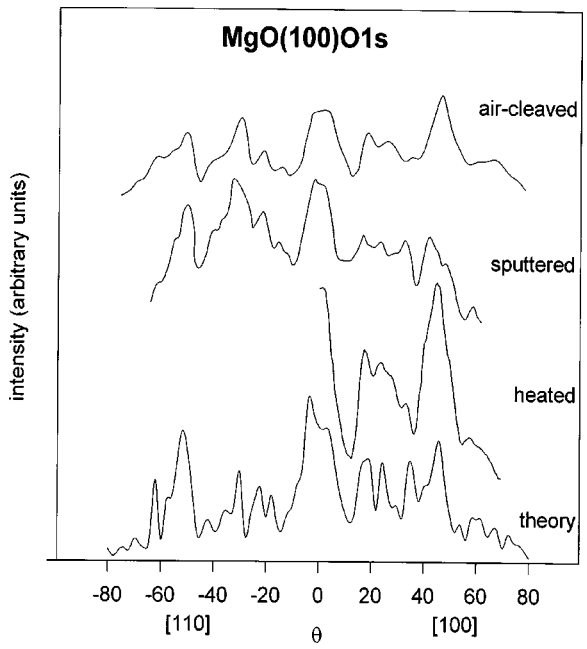

FIG. 2. Comparison of calculated O 1s photoelectron diffraction polar angle distributions along [100] and [110] azimuths from a MgO(001) surface, with experimental data sets from three different samples. The data from the air-cleaved and sputtered samples are from Ref. 12. Data from the heated sample are from Ref. 14.

culation is also based on a LEED package, in this case a major restructuring of the program is required—one that involves a significantly greater programming effort.

We have also performed a fully convergent calculation by the path-reversed algorithm, for 12 composite layers with two subplanes each, with interlayer multiple scattering calculated by the RFS scheme. No smoothing has been applied to the calculation to account for the effect of the data collection instrumentation. The calculated results are displayed at the bottom of Fig. 2 for comparison with three different sets of experimental data.[12,14] The upper two sets of data are from air-cleaved samples of MgO(001) with different methods of preparation. The first distribution is from a sample on which no sputtering has been performed. It appears that after sputtering there is less anisotropy in the azimuthal scan, indicating more surface disorder. The second distribution is from a sample which is sputtered and annealed at low temperature to remove surface contaminants. Some effect of the increase in disorder can be seen in the loss of intensity in the peak along the [100] direction at about $\theta = 45°$ as well as in the shifting of peak positions. The electron analyzer used in these experiments has an angular resolution of about $\pm 3°$. The third set of data is from a sample prepared only by heating to high temperature, and measured with a detector of higher angular resolution. While different in scale, it can be seen to resemble the first data set, but with more distinct features and different peak positions. The significant differences found among the three sets of experimental data for these azimuths indicate the photoelectron distribution from MgO(001) is quite sensitive to surface preparation. In light of these differences, the overall agreement with the simulations is quite satisfactory. The differences from experiment are found mainly in the range from $\theta = 20°$ to $\theta = 40°$, and around $\theta = 60°$, where significant differences among the experimental results are found.

IV. CONCLUSION

In conclusion, we have developed a path-reversed theory of core-level photoemission from ordered surfaces with more than one atom per unit cell. The calculations may be performed by a conventional LEED computer program, which needs to be modified only to extract the amplitudes of incoming spherical waves at each atomic emitter. If the interlayer scatterings are treated by the RFS method, only one run of the algorithm is needed to generate the spherical waves for all emitters and all initial states. This is in contrast with the conventional time-forward photoemission methods, which sum up scattering paths from each emitter and each initial state. In addition, the ease with which the current scheme for the generation of photoelectron diffraction can be implemented within conventional LEED codes makes the application of the many powerful approximations that have been developed within that discipline for automated structure determination [e.g., linear LEED (Ref. 15) and tensor LEED (Ref. 16)] straightforward.

We have shown that the results generated from the current algorithm are reliable, and agree with both time-forward results and the experimental data from MgO(001). The same formalism can be applied to cases like photoemission from disordered clusters or to automated structural searches using photoelectron diffraction. For the latter, only minor modifications to the time-forward algorithms[8] of the corresponding LEED formalism is required.

ACKNOWLEDGMENTS

D.K.S. acknowledges financial support from the U.S. National Science Foundation (Grant Nos. DMR-9815092 and DMR-9972958-001) and the U.S. Department of Energy (Grant No. DE-FG02-84ER45076).

[1] A. Liebsch, Phys. Rev. B **13**, 544 (1976).
[2] C.H. Li, A.R. Lubinsky, and S.Y. Tong, Phys. Rev. B **17**, 3128 (1978).
[3] R. Gunnella, F. Solal, D. Sebilleau, and C.R. Natoli, Comput. Phys. Commun. **132**, 251 (2000).
[4] M. Biagini, Phys. Rev. B **48**, 2974 (1993).
[5] X. Chen and D.K. Saldin, Comput. Phys. Commun. **112**, 67 (1998); G.R. Harp, Y. Ueda, X. Chen, and D.K. Saldin, *ibid.* **112**, 80 (1998); X. Chen, G.R. Harp, Y. Ueda, and D.K. Saldin, *ibid.* **112**, 91 (1998).
[6] H.S. Wu, C.Y. Ng, T.P. Chu, and S.Y. Tong, Phys. Rev. B **57**, 15 476 (1998).

[7] M.D. Pauli and D.K. Saldin, Phys. Rev. B **64**, 075411 (2001).
[8] P.J. Rous and J.B. Pendry, Comput. Phys. Commun. **54**, 137 (1989).
[9] J.B. Pendry, *Low Energy Electron Diffraction* (Academic, London, 1974).
[10] M.A. Van Hove and S.Y. Tong, *Surface Crystallography by LEED* (Springer, Heidelberg, 1977).
[11] S.Y. Tong and H.C. Poon, Phys. Rev. B **37**, 2884 (1988).
[12] S. Varma, X. Chen, J. Zhang, I. Davoli, D.K. Saldin, and B.P. Tonner, Surf. Sci. **314**, 145 (1994).
[13] J.B. Zhou, H.C. Lu, T. Gustafsson, and P. Haberle, Bull. Am. Phys. Soc. **38**, 279 (1993).
[14] D. Agliz, A. Quemerais, and D. Sebilleau, Surf. Sci. **343**, 80 (1995).
[15] A. Wander, J.B. Pendry, and M.A. Van Hove, Phys. Rev. B **46**, 9897 (1992).
[16] P.J. Rous, J.B. Pendry, D.K. Saldin, K. Heinz, K. Müller, and N. Bickel, Phys. Rev. Lett. **57**, 2951 (1986).